Mon. Not. R. Astron. Soc. **350,** 587–595 (2004) doi:10.1111/j.1365-2966.2004.07667.x

# High-speed Keck II and *RXTE* spectroscopy of Cygnus X-2 – I. Three X-ray components revealed by correlated variability

K. O'Brien,[1,2,3]★ Keith Horne,[2] Richard H. Gomer,[4] J. B. Oke[5,6] and M. van der Klis[3]

[1]*European Southern Observatory, Alonso de Cordova 3107, Santiago, Chile*
[2]*School of Physics and Astronomy, University of St Andrews, St Andrews KY16 9SS*
[3]*Astronomical Institute 'Anton Pannekoek', University of Amsterdam, Amsterdam 1098-SJ, the Netherlands*
[4]*Howard Hughes Medical Institute and Department of Biochemistry and Cell Biology, MS-140, Rice University, Houston, TX 77005-1892, USA*
[5]*California Institute of Technology, Mail Stop 105-24, Pasadena, CA 91125, USA*
[6]*Dominion Astrophysical Observatory, Herzberg Institute of Astrophysics, National Research Council of Canada, 5071 West Saanich Road, Victoria, BC V8X 4M6, Canada*

Accepted 2004 January 26. Received 2004 January 24; in original form 2002 January 17

**ABSTRACT**

We have performed simultaneous X-ray and optical spectroscopic observations of the low-mass X-ray binary Cygnus X-2. We have used a new data system attached to the Low Resolution Imaging Spectrograph (LRIS) instrument on Keck II to obtain spectra with a mean time resolution of 72.075 ms, simultaneous with pointed X-ray observations using the Proportional Counter Array (PCA) onboard *RXTE*. In this paper, we have analysed the variability in both wavebands on time-scales of 16 s. During our observations Cygnus X-2 covered all three branches of the Z-curve, allowing us to study how the changes in X-ray spectral state affect the optical emission. As the optical flux rises, the X-ray intensity first rises on the horizontal branch ($0 < S_z < 1$) but then falls on the normal branch ($1 < S_z < 2$) and flaring branch ($2 < S_z < 3$), where $S_z$ is a rank number characterizing the position on the Z-curve. This linear increase in the optical flux with $S_z$ indicates the optical flux is a good predictor of the accretion rate (possibly normalized by its own long-term average) inferred from the Z-state $S_z$. We have used this correlation to decompose the total X-ray count rate into three distinct spectral components.

**Key words:** binaries: close – stars: individual: Cyg X-2 – X-rays: binaries.

## 1 INTRODUCTION

Cygnus X-2 is one of the best studied low-mass X-ray binaries (LMXBs) as a result of its X-ray variability and observable optical counterpart. Cygnus X-2 is a close binary comprising a 1.78 $M_\odot$ neutron star in a 9.84 d binary orbit with a 0.6 $M_\odot$ subgiant companion star (Orosz & Kuulkers 1999). Since its discovery in 1965 (Bowyer et al. 1965) there have been a host of observations in the optical (e.g. van Paradijs et al. 1990), ultraviolet (e.g. Vrtilek et al. 1990) and X-ray (e.g. Kuulkers, van der Klis & Vaughan 1996) wavebands. The optical counterpart of Cygnus X-2, V1341 Cygni, has a spectral type A9 III and contributes approximately 50 per cent of the total visual flux (Casares, Charles & Kuulkers 1998). The reprocessing of X-rays in Cygnus X-2 is shown by the large contribution of the disc to the UV continuum and emission line fluxes, which arise predominantly from the X-ray heated accretion disc (de Jong, van Paradijs & Augusteijn 1996).

Cygnus X-2 belongs to the subclass of LMXBs known as Z-sources, whose X-ray spectral states trace a Z-shaped pattern in X-ray colour–colour diagrams (see Hasinger & van der Klis 1989). In a similar manner to the colour–colour diagrams familiar to optical astronomers, whose colour indices are magnitude differences between two bands, X-ray colour–colour diagrams employ hardness ratios, which are ratios of counts in a high-energy band to counts in a low-energy band. Typically a hard colour (hardness ratio for two high-energy bands) is plotted against a soft colour (hardness ratio for two low-energy bands). The X-ray equivalent of a colour–magnitude diagram is a hardness–intensity diagram, which plots a hardness ratio against the X-ray intensity (count $s^{-1}$) in some band. The location of the source in these diagrams provides information about changes in the shape of the X-ray spectrum and intensity, which arise for example from changes in the mass accretion rate on to the neutron star. In the case of the Z-sources, they seem to move smoothly along three distinct tracks, from the horizontal branch, the upper-most stroke, through the normal branch, the diagonal stroke, and on to the flaring branch, the lowest stroke, a sequence that until recently has been interpreted as a monotonic increase in the mass accretion rate from below to above the Eddington limit (Hasinger & van der Klis 1989). However, there is mounting evidence that this simple relationship is not the whole story and that a further parameter is needed to fully describe the X-ray behaviour. This

★E-mail: kobrien@eso.org

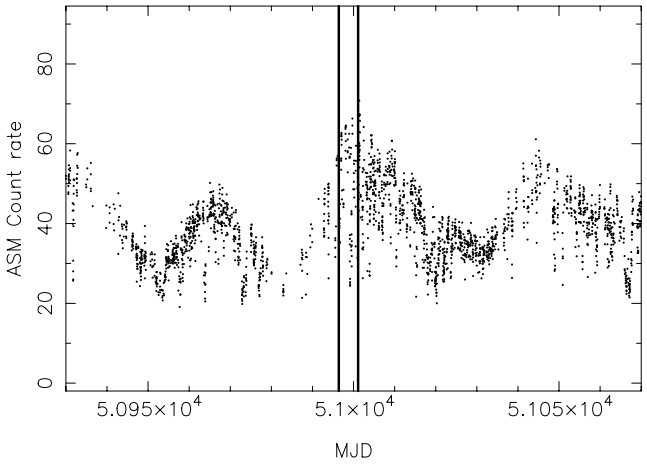


**Figure 1.** The *RXTE* All Sky Monitor light curve for Cygnus X-2. The vertical lines show the beginning and end of the Keck II and *RXTE* observations used in our analysis.

has been demonstrated most noticeably with the parallel lines phenomena, where the relationship between the X-ray luminosity and quasi-periodic oscillation (QPO) frequency is valid on short timescales only, but changes in the duration of days to weeks indicate a second parameter is needed to fully characterize the X-ray emission of LMXBs [see van der Klis (2001) for a discussion of this phenomenon].

The position of the Z in the X-ray colour–colour diagram and the shapes of the soft and hard colour–intensity diagrams evolve on a time-scale of weeks (Kuulkers et al. 1996). During this time Cygnus X-2 varies between three levels: high, medium and low, as defined by Kuulkers et al. (1996). The low intensity level is rare and only observed in the binary phase range 0.8–0.2, indicating it may be linked to a grazing eclipse of the X-ray emitting region by the mass donor star. More normally, the system appears to move slowly between the medium and high intensity levels. This can be seen in the *RXTE* All-Sky Monitor (ASM) light curve, a section of which is shown in Fig. 1. The source can be seen to move slowly between the medium level, with a count rate of $\sim 30$ count s$^{-1}$ and the high level where the count rate is $\sim 50$ count s$^{-1}$. However, large, short time-scale deviations from these levels can also be seen. These sudden drops in the count rate are caused by motion along the Z-curve and are not thought to be related to the longer time-scale changes (the so-called secular variations). The upper edge of this envelope represents the count rate at the hard vertex, between the horizontal and normal branches, where the count rate is highest.

Both the colour–colour diagrams and colour–intensity diagrams for the medium and high intensity levels are very different. In the high intensity level, the hard colour–intensity diagram shows linear, almost horizontal horizontal and flaring branches, whilst in the medium level these branches are more curved. The flaring branch is also truncated during the high level, which has been interpreted as obscuration by material in the binary, whereas in the medium level, the flaring branch intensity varies smoothly with the X-ray intensity. It is thought that the truncation is most noticeable in the flaring branch as it coincides with the highest mass accretion rate, which causes the inner disc to swell and shield our view of the X-ray emitting regions (see Kuulkers et al. 1996, for a more detailed description).

Cygnus X-2 exhibits Type I X-ray bursts (e.g. Kuulkers, van der Klis & van Paradijs 1995), confirming the presence of a neutron star, as seen in many other neutron star binaries, including the Z-source GX 17+2 (Kahn & Grindlay 1984; Kuulkers et al. 1997). These bursts typically have rise times of 0.1–10 s and are thought to be the result of thermonuclear burning of accreted material on the surface of the neutron star (Smale 1998). Unlike neutron stars, black holes have no stellar surface and Type I X-ray bursts are not observed. There is also tentative evidence for a third periodicity in Cygnus X-2 with a period of 78 d, although the interpretation of this is complicated by the changes in X-ray flux as Cygnus X-2 moves around the colour–colour diagram. The long-term quasi-periodicity can be seen in Fig. 1, where the peak-to-peak separation is $\sim$30–40 d. Wijnands, Kuulkers & Smale (1996) associate this periodicity with that of a precessing accretion disc, as seen in Hercules X-1 (Giacconi et al. 1973).

A previous multiwavelength campaign on Cygnus X-2 during 1988 June and October, involving X-ray (Hasinger et al. 1990), UV (Vrtilek et al. 1990), optical (van Paradijs et al. 1990) and radio (Hjellming et al. 1990) observations, revealed many interesting features of the correlated variability, which are summarized schematically in fig. 9 of Hasinger et al. (1990). They found that there was a direct correlation between the UV and optical fluxes and the position on the Z-diagram, although the sampling of the optical and UV data ($\sim$100s of seconds) only allowed general trends to be observed. They also found a more complicated behaviour between the X-ray intensity and the position on the Z-diagram. In this series of papers we will build upon these observations, with higher time resolution optical data ($\sim$ seconds), which enable us to observe the previously observed trends in much more detail.

In this paper, the first in the series, we shall discuss the observations of the X-ray and optical spectral variability of Cygnus X-2 in terms of broad-band variability on time-scales of $10^{2-5}$ s. We will also go into some depth into the data reduction tasks performed, which will be abridged in subsequent papers. In subsequent papers, we will discuss the variability of narrow-band features in the optical spectra and how this is affected by the X-ray spectral state. We will also discuss a simultaneous timing analysis of the data and the nature of the rapid ($\sim$ seconds) correlated X-ray and optical variability in terms of the time delayed optical emission relative to the driving X-ray variability.

## 2 DATA

Simultaneous Keck II and *RXTE* observations of Cygnus X-2 were taken during UT 1998 July 2–6 as part of our campaign to search for correlated optical and X-ray variability in X-ray binaries. In this paper, we will show the optical data from the first and last nights of our campaign, when atmospheric conditions were most favourable. An analysis of the entire X-ray data set showed that using only this subset did not reduce our coverage of the different spectral states of Cygnus X-2.

### 2.1 Optical

The optical data were taken using the Low Resolution Imaging Spectrograph (LRIS; Oke et al. 1995) on the 10 m Keck II telescope on Mauna Kea, Hawaii. A summary of the observations is given in Table 1. The LRIS was used with a 5.2 arcsec slit masked with aluminized mylar tape to form a square aperture. The 300/5000 grating used has a mean dispersion of 2.55 Å pixel$^{-1}$ in the range 3600–9200 Å.

We used a novel data acquisition system, which reads out the CCD continuously, to obtain more than 220 000 spectra of Cygnus

**Table 1.** Summary of the Keck II optical observations. The binning factor of 14 used in the light curves gives an integration time of 1.01 s for the resulting spectra.

| File name | Observation | Night | *RXTE* window | UT at start | Elapsed time (s) | Number of unbinned spectra |
|---|---|---|---|---|---|---|
| K0010 | A | 1 | 1 | 10:48, 1998 July 02 | 1654 | 23 268 |
| K0013 | B | 1 | 2 | 13:15, 1998 July 02 | 3930 | 58 086 |
| K4005 | C | 5 | 1 | 09:08, 1998 July 06 | 1460 | 20 230 |
| K4007 | D, E | 5 | 2, 3 | 10:05, 1998 July 06 | 3890 | 46 942 |
| K4009 | F | 5 | 4 | 11:42, 1998 July 06 | 3746 | 51 926 |
| K4011 | G | 5 | 5 | 13:17, 1998 July 06 | 1710 | 23 842 |

X-2, in the form of continuous byte streams lasting typically 50 min. The mean integration time was measured to be 72.075 ms and there is no dead time between individual spectra.

In addition to the 2048-pixel spectrum, 25-pixel under-scan and 75-pixel over-scan regions were used to measure the CCD bias level, which we subtracted from each spectrum. The noise for a given pixel was calculated using a readout noise of 6.3 $e^-$ and a gain of 4.7 $e^-$ $ADU^{-1}$. Cosmic rays were rejected with a threshold of $10\sigma$ from the de-biased frames. A master flat-field image was created by finding the median of 700 individual flat-field spectra. This image showed no deviations above 0.3 per cent in all but three pixels. It was decided that it was therefore not necessary to flat-field individual spectra. Calibration arc spectra and spectra of the sky in the region of the object were taken at regular intervals.

The background spectrum, which accounts for ∼0.9 per cent of the total flux, contains two components: one from scattered light within the spectrograph and a second from the sky brightness. The scattered light level was measured from the counts in the pixels below 3400 Å, where both the GRISM and atmospheric transmission are negligible. This level was removed from all spectra and then the sky spectrum was subtracted using the best fit to spectra taken of a blank sky field. These sky spectra were taken at the beginning and end of the exposure, so that long time-scale variations could be detected. The mean and variable components of these spectra were found by creating a light curve for each pixel and extracting the mean and gradient of this light curve. In order to suppress the pixel-to-pixel variations, the mean and gradient were then averaged in wavelength, with a running median filter of width 101 pixels. The gradient in time of the data was found to be consistent with zero, indicating that the spectrum was constant for the duration of the exposure (∼50 min). This spectrum is more than a simple sky spectrum and contains both the spectrum of the sky background and an additional component thought to be the result of scattered light within the spectrograph.

The wavelength calibration was accomplished by fitting a second-order polynomial to seven lines in a median spectrum of exposures of Hg and Ar arc lamps. Arc spectra from the beginning and end of the run were used to take into account any drifts in the wavelength scale. The wavelength calibration was applied using the MOLLY spectral analysis package.

The individual spectra of Cygnus X-2 were flux calibrated using exposures taken of the standard star Feige 67 (Oke 1990). We fitted a low-order polynomial to the median spectrum of the observations of this standard star. The resulting fit was used as a flux calibration and again applied using MOLLY. The average spectrum from observation G is shown in Fig. 2. Several emission and absorption features can be clearly seen and will be described in detail in Paper II.

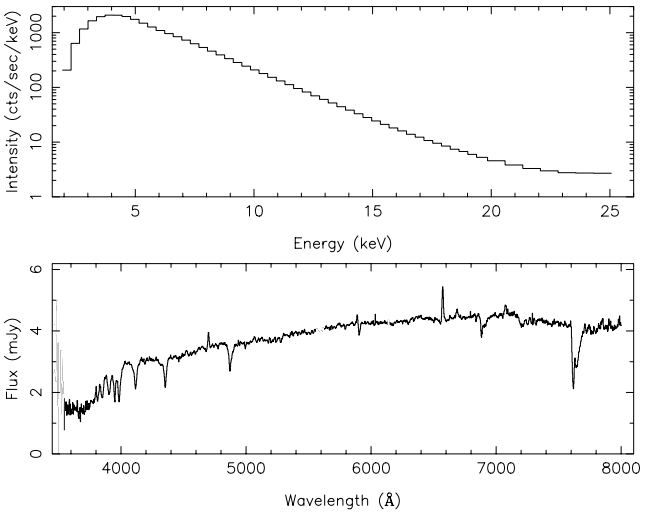


**Figure 2.** The average X-ray (top panel) and optical (bottom panel) spectra from observation G. The X-ray spectrum is plotted with a logarithmic scale.

### *2.1.1 Time calibration*

As a result of the nature of the continuous stream of data, it was impossible to attach accurate time marks to each individual spectrum. Individual time marks were placed after every other spectrum using the computer clock. In order to establish an absolute time reference, secondary time stamps were obtained on many occasions during the five night observing run. To create these time stamps, an incandescent lamp that illuminated the CCD was modulated in synch with WWVH time signals. From these time stamps we found an ephemeris for the observation and the mean exposure time. These were checked against the computer's time marks and found to be in excellent agreement.

The input times were corrected to the Solar system barycentre, using the subroutines supplied by the International Astronomical Union (IAU) working group on Standards Of Fundamental Astronomy (SOFA[1]). Finally, these times were converted to seconds since JD 245 0996.0, in order to make the numbers more manageable.

In order to increase the signal-to-noise ratio of the individual spectra and make the data set more manageable, the spectra were binned in time by a factor of 14 to give 1646 binned spectra with a time resolution of 1.01 s.

[1] http://www.iau-sofa.rl.ac.uk/

### 2.2 X-ray

The X-ray data taken with the Proportional Counter Array (PCA) onboard the *RXTE* satellite covered 42 ks of exposure time during UT 1998 July 2–6. We have used a subset of this data, which amounts to 20.3 ks and represents the times of simultaneous coverage during favourable atmospheric conditions. During this time all five PCUs were switched on. The data were analysed using the FTOOLS v5.1 software suite. The STANDARD-2 mode data were used with a time resolution of 16 s to create colour–colour and hardness–intensity diagrams, and to study the simultaneous variability. The light curves were extracted, using FTOOLS package SAEXTRCT, in four energy ranges, using the STANDARD-2 channels 1–5, 6–12, 13–21 and 22–39. This corresponds to 1.94–3.72, 3.72–6.22, 6.22–9.46 and 9.46–16.02 keV. The times were corrected to the Solar system barycentre using the FTOOLS package FAXBARY. The minimum count rate of 4000 count $s^{-1}$ implies that background subtraction was not necessary. The dead time is estimated to be <2 per cent, which is smaller than the variability we are studying and therefore a dead time correction was not applied to the X-ray light curves. The average spectrum during observations G is shown in Fig. 2.

The broad-band X-ray spectral variations of Z-sources are most clearly shown in an X-ray colour–colour diagram. These are shown for Cygnus X-2 in, e.g. Wijnands & van der Klis (2001). The colour–colour and hardness–intensity diagrams presented by them contain data from the five nights of observations. In this paper we present

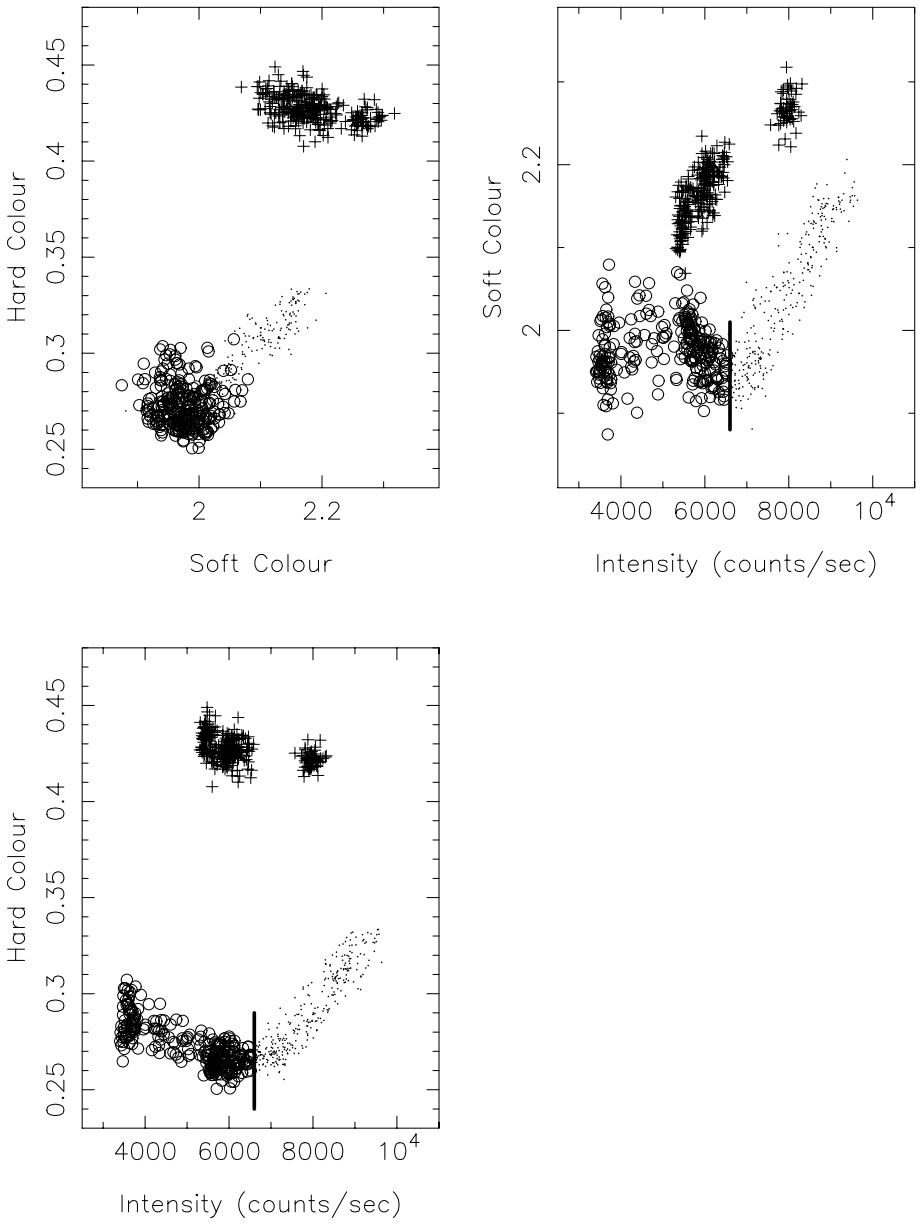


**Figure 3.** Top left, X-ray colour–colour diagram for Cygnus X-2, based on the *RXTE* PCA data between UT 1998 July 1–6. The data are taken from the STANDARD-2 mode, with a time resolution of 16 s. The soft colour is defined as the ratio of the intensities in the ranges 1.94–3.72 and 3.72–6.22 keV. The hard colour is the ratio of the intensities in the ranges 6.22–9.46 and 9.46–16.02 keV (an increase in colour means the spectrum hardens). Bottom left, the hardness–intensity diagram for the hard colour and the total intensity. Top right, the hardness–intensity diagram for the soft colour and the total intensity. The horizontal, normal and flaring branches are indicated by pluses, dots and open circles, respectively. The vertical line shows the X-ray intensity at the normal/flaring branch vertex.

a subset of this data for which we have simultaneous optical observations. The colour–colour diagram from our *RXTE* observation is shown in Fig. 3. The soft colour is defined as the intensity in the range 3.72–6.22 keV, divided by the intensity in the range 1.94–3.72 keV. The hard colour is similarly defined as the intensity in the range 9.46–16.02 keV divided by the intensity in the range 6.22–9.46 keV.

## 3 THE BROAD-BAND X-RAY SPECTRAL CHANGES

In Fig. 3, Cygnus X-2 can clearly be seen to trace out all three branches of the Z-curve, beginning on the horizontal branch during the first night, then moving on to the lower normal branch and the flaring branch during the last night. If motion along the Z is the result of changes in the mass accretion rate (see Hasinger et al. 1990), we would infer that $\dot{M}$ increases from night to night.

The hardness–intensity diagrams, which plot the X-ray colour changes as a function of intensity, show that the hard colour varies smoothly with intensity whilst on a given branch, as expected from previous observations of the source. The transition between the normal branch and the flaring branch, referred to as the soft vertex, is clearly seen, but the horizontal branch to normal branch transition region, referred to as the hard vertex, is not covered in any of our observations.

The soft colour–intensity diagram also shows a linear trend on the horizontal and normal branches. This is interpreted as changes in the X-ray production mechanism as a function of the increasing mass accretion rate. The soft colour–intensity diagram deviates from the expected linear relationship (see e.g. Kuulkers et al. 1996) whilst on the flaring branch. The colour–intensity diagrams are characteristic of the high intensity level colour–intensity diagram described by Kuulkers et al. (1996), exhibiting an almost horizontal flaring branch in the hard colour–intensity diagram.

## 4 THE SIMULTANEOUS X-RAY AND OPTICAL VARIABILITY IN CYGNUS X-2

### 4.1 General features of night 1, UT 1998 July 1–2

The simultaneous X-ray and optical observations of Cygnus X-2 from night 1 of our observations are shown in Fig. 4. The position in the X-ray colour–colour diagram (the pluses in Fig. 3) show that Cygnus X-2 was on the horizontal branch throughout the night. It began the night near the hard vertex, but by the end of the night had moved along the horizontal branch away from the hard vertex, which coincides with the lowest X-ray and optical fluxes. During these observations there is a general correlation between the X-ray and optical flux. In contrast to the normal and flaring branch light curves shown in Fig. 5 and described in the next section, no rapid ($10^{0-2}$ s) correlated variability is seen on the horizontal branch. Even the X-ray burst observed around $t = 93\,000$ s shows no optical counterpart. (Correlated, time-delayed variability on these time-scales will be analysed in a subsequent paper in this series.)

### 4.2 General features of night 5, UT 1993 July 5–6

At the beginning of night 5, Cygnus X-2 was on the flaring branch. During the night it moved off the flaring and on to the normal branch, finishing approximately half-way between the soft and hard vertices. The overall X-ray intensity is now anticorrelated with the optical flux, as shown in Fig. 5. Although this might seem surprising, it is in fact the same behaviour as reported by Hasinger et al. (1990) between the X-ray intensity and UV flux. Their interpretation for this

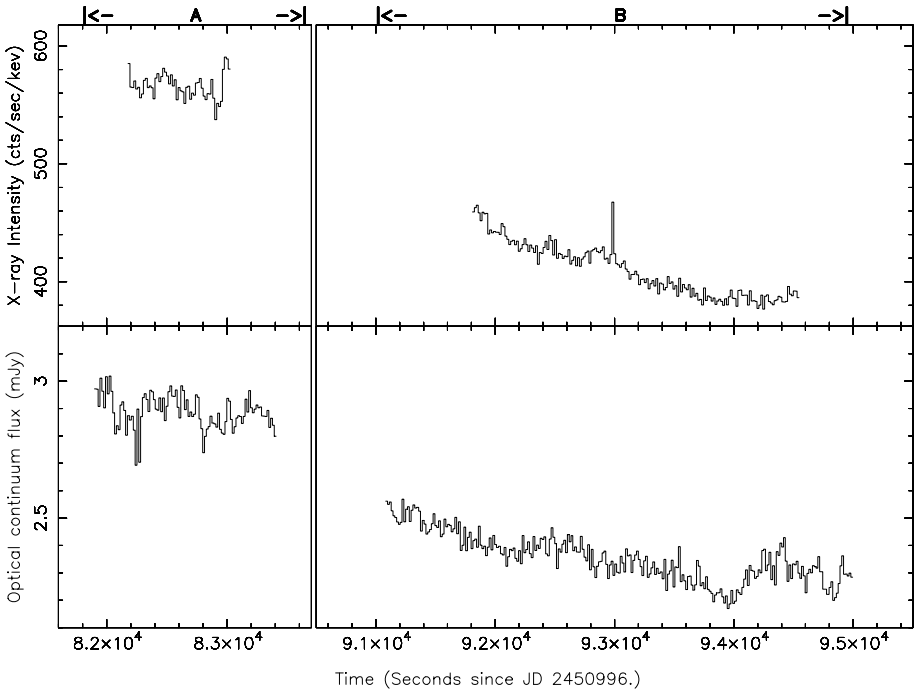


**Figure 4.** Top panels, the total X-ray intensity during the two *RXTE* visits (labelled A and B) from night 1. Bottom panels, the optical continuum flux in the range 5000–5800 Å . The time is seconds elapsed since JD 245 0096.0, the beginning of the night. The time resolution of the light curves is 16 s. The relative sizes of the left and right panels have been chosen to keep the scale the same for both light curves. The X-ray burst can clearly be seen at $t = 93\,000$ s, with no optical counterpart.

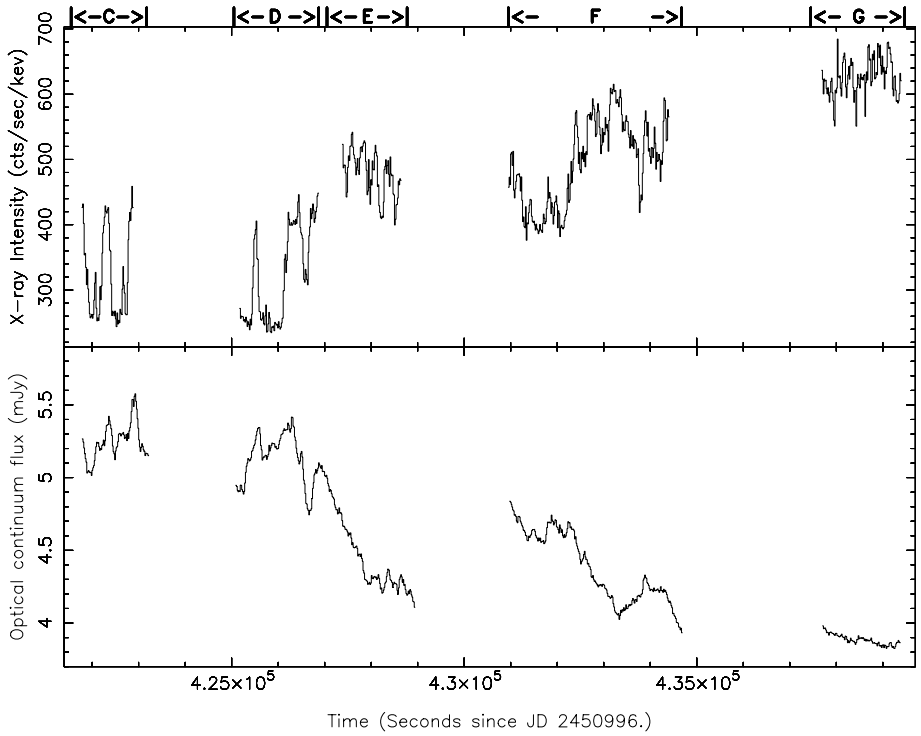


**Figure 5.** Top panel, the total X-ray intensity during the five *RXTE* visits (labelled C–G) from night 5. Bottom panel, the optical continuum flux in the range 5000–5800 Å. The time is seconds elapsed since JD 245 0996.0, the beginning of the first night of the run. The time resolution of the light curves is 16 s.

was that the reprocessing material in the disc, which gives rise to much of the observed optical/UV emission, intercepts X-rays from a number of different lines of sight, whereas our observations are limited to the line of sight from the neutron star to the detector. As these lines of sight may have quite different fluxes, averaging over many of them gives a better indication of the bolometric X-ray flux and hence $\dot{M}$. They note that the observed X-ray flux is sensitive to both the changing spectrum of the source and any anisotropy in the X-ray emission. Perhaps the existence of anisotropic emission could also explain the lack of an optical counterpart to the X-ray burst, as the burst is seen by the observer, but not the region of the binary responsible for reprocessing the X-ray photons into optical/UV photons.

## 5 THE CORRELATIONS BETWEEN THE X-RAY AND OPTICAL DATA

In Fig. 6 we plot the X-ray intensity in the soft (top panel) and hard (bottom panel) bands as a function of the optical continuum flux. A striking feature is the significant range in X-ray intensity $I_{\rm X}$ that occurs at each optical flux (the error bars are typically smaller than the markers in the plot). This indicates there is not a simple one-to-one relationship between the X-ray and optical fluxes of Cygnus X-2. The range over which $I_{\rm X}$ varies, at a given optical flux ($F_\nu$), remains rather small on the horizontal branch (shown as pluses in Fig. 6), but it then increases dramatically as the system progresses up the normal and flaring branches (marked by dots and open circles, respectively). It appears plausible from Fig. 6 to define smooth upper and lower envelopes representing the extreme values of $I_{\rm X}$ that occur at each optical flux. These envelopes are indicated by the solid and dashed lines in Fig. 6.

On the basis of the optical and X-ray variability exhibited in Fig. 6, we investigate here a decomposition of the X-ray intensity $I_{\rm X}$ into

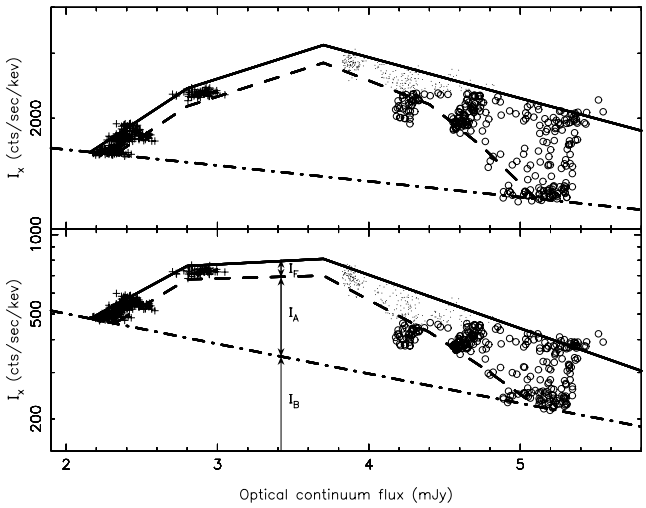


**Figure 6.** Top, a plot of the logarithm of the soft X-ray intensity (1.94–6.22 keV) versus optical continuum flux. Bottom, the same plot for the hard X-ray intensity (6.22–16.02 keV). The solid, dotted and dot-dashed lines represent the limits of the three components described in the text. The normal, horizontal and flaring branch points are represented by pluses, dots and open circles, respectively.

three spectral components, $I_{\rm F}$, $I_{\rm B}$ and $I_{\rm A}$, where the subscripts stand for flaring, baseline and accretion respectively (see Section 5.1). This decomposition can be expressed mathematically as

$$I_{\rm X}(F_\nu) = \alpha(t) I_{\rm F}(F_\nu) + I_{\rm B}(F_\nu) + I_{\rm A}(F_\nu), \quad (1)$$

where $\alpha(t)$ is a coefficient to describe the variability in $I_{\rm F}$, with $0 \leqslant \alpha(t) \leqslant 1$. The three components are discussed below and shown schematically in the lower panel of Fig. 6.

### 5.1 The three components

The first component, $I_F$, is associated with the rapid variation between the bounds of the envelope. The variability of this component is mimicked in the optical light curve, as can be seen in the correlated flares and dips during observations C and D, shown in Fig. 5. In other words, on the normal and flaring branches, the area between the full and dashed lines in Fig. 6 is filled in by the source performing diagonal (correlated) strokes on the time-scale of $10^{1-2}$ s.

A second interesting feature in Fig. 6 is the lower envelope or baseline in the range of $I_X$ when $F_\nu > 4.8$ mJy. This baseline in X-ray intensity is visited repeatedly by the system during observations C and D in Fig. 5, where it appears to represent a level below which $I_X$ never goes. We notice in Fig. 6 that this floor in $I_X$ decreases as the optical flux rises. Furthermore, if we extrapolate that slope to lower optical flux it appears to predict the lowest $I_X$ we observed on the horizontal branch, at $S_z = 0$. We therefore draw a line across the diagram and identify the X-ray intensity of this baseline component as $I_B$, where $I_B$ decreases linearly as the optical flux rises.

The third component is simply the difference between the baseline intensity $I_B$ and the lower envelope of $I_X$ at each optical $F_\nu$. This component first increases along the horizontal branch, and then decreases along the normal and flaring branches. We refer to the X-ray intensity of this component that varies smoothly with the optical flux as $I_A$ because we suggest that it is related to the accreted material (see discussion).

Our decomposition is somewhat arbitrary. For example, we could combine $I_B$ and $I_A$ into a single component with a more complex dependence on optical flux. However, as described above, we believe that the morphology of the optical and X-ray variations, especially the apparent floor in the $I_X$, provides sufficient motivation to further explore our proposed three-component decomposition.

There are several deviations outside this envelope, which we will describe on a case-by-case basis. The most obvious of these deviations occurs around $F_\nu = 4.3$ mJy, where $I_X$ is below the lower edge of the envelope. This deviation can be seen in the X-ray light curve in Fig. 5 around $t = 434\,000$ s in the form of a dip in the X-ray light curve that has no optical counterpart. Such non-correlated dips have been seen previously in Cygnus X-2 (Kuulkers et al. 1996) and interpreted as momentary obscuration by material along the line of sight to the neutron star. They are not expected to have an analogue in the optical light curve as the line of sight from the X-ray emitting region to the reprocessing region is different from the direct line of sight for the observer. Similar non-correlated dips are seen in the flaring branch observations, which result in the dips seen around $F_\nu = 4.2$ mJy, where the X-ray intensity drops to the lower, floor level (described in the next section).

Another deviation, seen at the highest optical fluxes, is associated with the reprocessed flares seen during observation C in Fig. 5. While we would expect such correlated flares to remain within the envelope, as they do appear to have X-ray analogues, we have not taken into account the time delay between the X-ray and optical emission. This time delay, which will be quantified in another paper in this series, is most noticeable when the amplitude of the variability is largest on time-scales similar to the time resolution of the data, as is the case on the flaring branch. This rapid variability can cause spurious correlations, as is the case here.

The variability outside of the envelope at low optical fluxes $F_\nu =$ 2.1–2.2 mJy is not understood and more data will be needed in order to determine the cause of the non-correlated variability.

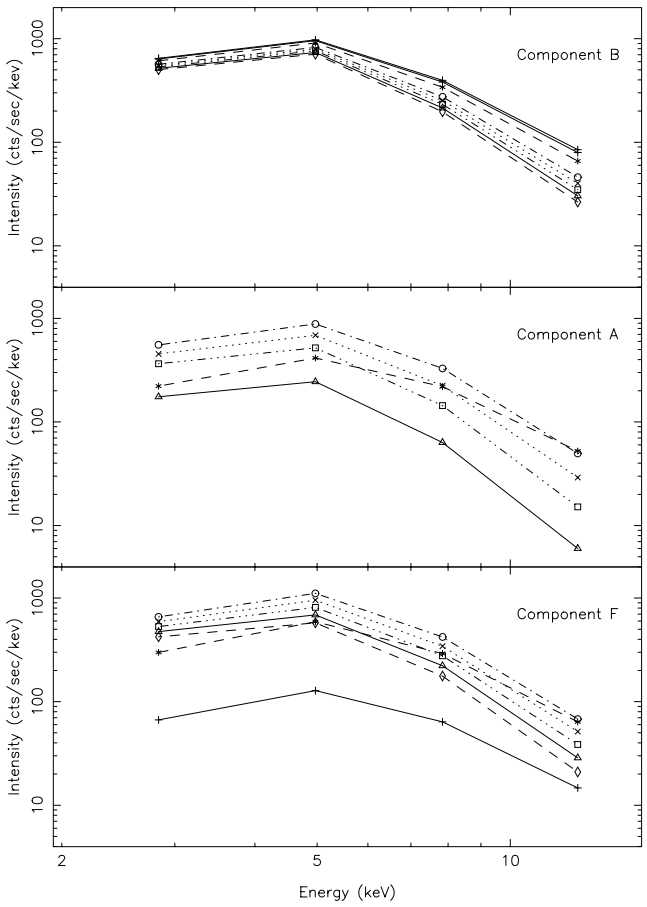


**Figure 7.** The spectra of the three identified components in the X-ray spectra. The components are $I_B$, $I_A$ and $I_F$ from top to bottom panel, respectively. The spectra were calculated when the optical continuum flux equalled 2.3 (pluses, solid line), 2.8 (stars, dashed line), 3.7 (circles, dot-dashed line), 4.05 (crosses, dotted line), 4.4 (squares, dot-dot-dot-dashed line), 4.75 (triangle, solid line) and 5.1 (diamond, dashed line). The spectra for $I_A$ when $F_\nu = 2.3$ and 5.1 are set to zero, as can be seen from Fig. 6.

### 5.2 The spectra of the components

Comparing the upper and lower panels of Fig. 6, showing the relationship between the X-ray and optical fluxes for the soft and hard X-ray bands, respectively, we see how the three components depend on the X-ray band. The most striking feature of this is how the hard X-ray intensity (lower panel) reaches its maximum at lower $F_\nu$ than the soft X-ray intensity.

In order to determine the spectrum of each component and how it varies with the optical flux, we have subdivided the X-ray band into a total of four bands. These bands are the same as those chosen to create the hardness ratios shown in Fig. 3, namely 1.94–3.72, 3.72–6.22, 6.22–9.46 and 9.46–16.02 keV. The results of this decomposition are shown in Fig. 7. $I_B$ (top panel) is seen to have a roughly constant soft X-ray flux, while the hard X-ray flux drops steadily, leading to an overall softening of the spectrum. This is in contrast to $I_F$ (bottom panel), where the soft flux varies most. $I_A$ shows the least spectral variability, showing only a change between the transition from the horizontal to normal branch.

## 6 SUMMARY AND DISCUSSION

We have obtained a unique data set from Keck II and *RXTE* and used it to investigate the simultaneous X-ray and optical variability

in Cygnus X-2. We have found that on time-scales of $\sim 10^{2-5}$ s, the X-ray and optical variability show a positive correlation on the horizontal branch, changing to an anticorrelation on the normal and flaring branches.

However, on short time-scales, $\sim 10^{0-2}$ s, the optical light curves show correlated, yet time-delayed features of the X-ray light curves. This is as expected in a linear reprocessing model. (The short time-scale correlated variability will be discussed in more detail in a later paper.) The simultaneous X-ray and optical fluxes show a complicated correlation. Initially, whilst on the horizontal branch they show a fairly tight correlation. Then when Cygnus X-2 is on the normal branch, the X-ray and optical flux changes become anticorrelated, whilst still exhibiting a strong correlation. Then around the middle of the normal branch, the correlated variability changes again: the correlation becomes weaker with large changes in both the X-ray and optical variability.

We have used the simultaneous X-ray intensity and optical flux measurements to characterize the spectrum in terms of the three components $I_{\rm B}$, $I_{\rm A}$ and $I_{\rm F}$. It is clear that there are different phases in the behaviour of Cygnus X-2, represented by the different branches of the colour–colour diagram. This would appear to represent the complex interdependence of more than one component of the X-ray emission.

(i) Component $I_{\rm B}$. As stated earlier, $I_{\rm B}$ appears to describe the lowest possible X-ray intensity, or baseline as function of the rank number, $S_z$. The intensity is seen to fall to this level, but not below it, at both extremes of the Z-curve and possibly when the neutron star is momentarily obscured by intervening material. Component B smoothly softens between the observations on the horizontal and flaring branches, as a result of a drop in intensity, predominantly in the hardest energy range.

(ii) Component $I_{\rm A}$. The spectral shape of $I_{\rm A}$ remains constant while on the horizontal branch and also, with a different slope, on the normal and flaring branches, only changing in flux while on either branch. The spectrum is seen to change between the horizontal and normal or flaring branches, when the sense of the correlation changes, with a harder spectrum on the horizontal branch. Like $I_{\rm B}$, this component is relatively constant on time-scales of $10^{2-3}$ s. However, when the intensity drops into this region during non-correlated X-ray dips it does vary on these time-scales.

(iii) Component $I_{\rm F}$. $I_{\rm F}$ was defined such that it contains most of the $10^{1-2}$ s variability, as expressed by $\alpha(t)$ in equation (1). The instantaneous X-ray intensity appears to change randomly within its envelope, except during X-ray bursts and non-correlated dips, which we therefore do not associate with variations in $I_{\rm F}$. The spectrum of this component shows a highly variable soft intensity, so that the total spectrum softens with increasing $S_z$.

$I_{\rm F}$, which represents the rapidly varying material is the softest of the three components and could be associated with material in a hot inner disc. At a given optical flux and hence inferred mass transfer rate, the flux in this component varies rapidly and appears to drive much of the rapid optical response, as can be seen by the correlated X-ray and optical flares in observations C and D. Such rapid variability could be associated with inhomogeneities in the accretion flow.

$I_{\rm A}$, whose flux varies considerably, but with little change in the spectrum may be associated with the emission from the surface of the neutron star. Such variability could then be caused by the changing obscuration of the inner regions of the accretion flow by optically thick material.

However, no complete physical interpretation of the decomposition is possible as yet. This is particularly evident when considering $I_{\rm B}$, which represents the lowest (baseline) level and is the spectrum of the source when the accretion rate is at its lowest and highest levels. At these times there will be contributions from many regions within the binary, leading to a complicated spectrum. This component may include the non-thermal emission, which has been observed to increase with decreasing $\dot{M}$. Observations of similar variability of the so-called hard tail in Cygnus X-2 (Di Salvo et al. 2002) and other Z-sources would appear to support the existence of this variable hard component (Di Salvo et al. 2000; Frontera et al. 1998). In addition to this, it has been observed that the radio emission, which is linked to the mass outflow from the system, possibly in the form of a jet (Fender & Hendry 2000), is greatest at the lowest $S_z$ (Penninx et al. 1988) and hence optical flux, as seen in our observations.

The limited amount of data makes it impossible to assess the importance of effects such as the binary phase and the long-term periodicity on $I_{\rm A}$ and indeed the other two components. However, it is intriguing that such a simple decomposition leads to three distinct components that are suggestive of the three regions thought to affect the X-ray emission in neutron star X-ray binaries.

## ACKNOWLEDGMENTS

The authors thank John Cromer for writing, testing and loading the software that allowed the LRIS CCD to read out continuously, and Bob Leach for helpful discussions. The authors especially thank Tom Bida and Frederic Chaffee for their kindly letting us make changes to the LRIS system. The optical data presented herein were obtained at the W. M. Keck Observatory, which is operated as a scientific partnership among the California Institute of Technology, the University of California and the National Aeronautics and Space Administration. The observatory was made possible by the generous financial support of the W. M. Keck Foundation. This research has made use of NASA's Astrophysics Data System Abstract Service.

## REFERENCES

Bowyer S., Byam E., Chubb T., Friedmann H., 1965, Sci, 17, 894
Casares J., Charles P., Kuulkers E., 1998, ApJ, 493, L39
de Jong J. A., van Paradijs J., Augusteijn T., 1996, A&A, 314, 484
Di Salvo T. et al., 2000, ApJ, 544, L119
Di Salvo T. et al., 2002, A&A, 386, 535
Fender R. P., Hendry M. A., 2000, MNRAS, 317, 1
Frontera F. et al., 1998, in Scarsi L., Brandt H., Giommi P., Fiore F., eds, The Active X-ray Sky: Results from *BeppoSAX* and *RXTE*. Elsevier, Amsterdam, p. 286
Giacconi R., Gurksy H., Kellogg E., Levinson R., Schreier E., Tananbaum H., 1973, ApJ, 184, 227
Hasinger G., van der Klis M., 1989, A&A, 225, 79
Hasinger G., van der Klis M., Ebisawa K., Dotani T., Mitsuda K., 1990, A&A, 235, 131
Hjellming R. M., Han X. H., Cordova F. A., Hasinger G., 1990, A&A, 235, 147
Kahn S. M., Grindlay J. E., 1984, ApJ, 281, 826
Kuulkers E., van der Klis M., van Paradijs J., 1995, ApJ, 450, 748
Kuulkers E., van der Klis M., Vaughan B., 1996, A&A, 311, 197
Kuulkers E., van der Klis M., Oosterbroek T., Van Paradijs J., Lewin W. H. G., 1997, MNRAS, 287, 495
Oke J. B., 1990, AJ, 99, 1621
Oke J. B. et al., 1995, PASP, 107, 375

Orosz J. A., Kuulkers E., 1999, MNRAS, 305, 132
Penninx W., Lewin W. H. G., Zijlstra A. A., Mitsuda K., van Paradijs J., 1988, Nat, 336, 146
Smale A. P., 1998, ApJ, 498, L141
van der Klis M., 2001, ApJ, 561, 943
van Paradijs J. et al., 1990, A&A, 235, 156
Vrtilek S., Raymond J., Garcia M., Verbunt F., Hasinger G., Kurster M., 1990, A&A, 235, 162
Wijnands R., van der Klis M., 2001, MNRAS, 321, 537
Wijnands R. A. D., Kuulkers E., Smale A. P., 1996, ApJ, 473, L45

This paper has been typeset from a TEX/LATEX file prepared by the author.